PAPER

Check for updates

Novel synthesis of a self-healing Ce based eco-friendly sealing coating to mitigate corrosion in insulators installed in industrial regions

Simpy Sanyal,[a] Taeyong Kim,[a] Matheus Rabelo,[b] Duy Phong Pham*[a] and Junsin Yi [ID] *[c]

Overcoming hardware corrosion for high voltage insulators is a vital issue to prevent the sudden breakdown of insulators. The development of an efficient, economical, and eco-friendly anti-corrosion coating is essential to replace existing carcinogenic and toxic silicone-based coatings used by insulator industries. This article investigates the anticorrosion performance of a novel cerium-based sealing coating for insulator pins installed in highly corrosive (35 μm per year) industrial regions. The coating bath parameters were optimized to improve the self-healing, thermal, crack, and corrosion resistance of the coating. After immersion in a 60 000 ppm $CeCl_3 \cdot 7H_2O$ sealing coating bath for 60 minutes, a Ce-rich and dense protective coating (24.4 μm) is formed on the pin surface. The specimens immersed in a 60 000 ppm Ce sealing coating bath for 60 minutes show the lowest I_{corr}. The anticorrosion performance is enhanced by 95% for coated pins than non-coated ones. The electrochemical experiments, macroscopic and microscopic structural analysis confirm the anticorrosion performance of Ce-based sealing coatings for high voltage insulator pins. This work will facilitate a new branch of eco-friendly coatings for insulator and power industries.

1. Introduction

Insulators are one of the vital electrical elements in power utility. The entire reliability of the electrical installation depends on insulators. The ceramic insulator has been used since its invention for 150 years. The porcelain insulator has demonstrably higher resistance to degradation, electrical strength, and thermal resistance compared to its non-ceramic counterpart.[1] Corrosion of porcelain insulators has proved to be a significant threat to the secure and steady performance of power utilities. The losses resulting from corrosion are considered to be 2–5% of the gross national product of any country. The pin corrosion results in degradation of pin cross-sectional zone and interfacial strength between the pin and cement, which reduces the mechanical strength of the pin. Even corrosion products surrounding the pin may enhance hoop stress in the head of the insulator which results in cracking of the dielectric shell. This situation leads to the sudden failure of insulators and thus arise safety issues for power industries.[2] Fig. 1 depicts insulators collected from Yeongnam Naeryuk,

Southern coastal and Capital region industrial area of Korea with the same installation time, but varying corrosion rate from 10–35 μm per year. Fig. 1(a) shows the initiation of corrosion in the insulator pin. However, Fig. 1(b) and (c) depict the critical level of localized and surface corrosion in the insulator pin, even if all specimens share the same installation time. Fig. 1(d) presents the after-effect of pin corrosion. Insulator hardware mostly avails galvanized metal parts on account of their successful history of corrosion resistance in almost all polluted sites. In industrial sites, a severely contaminated environment exacerbates the risk of corrosive attack for insulators. The corrosion rate varies due to change in concentration of pollutants, temperature, and pH of rainfall for various industrial sites. The major pollutants found in industrial sites in Korea are SO_x, NO_x, and Cl. The concentration of SO_x, NO_x and Cl vary in the range of 0.54–4.7 μg m^{-3}, 0.95–3.03 μg m^{-3}, and 3.26–4.47 μg m^{-3} respectively in the atmosphere. The pH of rain varies in the range of 3.2–5.1 in extremely polluted industrial sites of Korea.[3–5] Under continuous exposure to an industrial environment, the galvanized film of the insulator pin would be transformed into other atmospheric products rapidly. These corrosion rates would be faster enough to cover galvanized surfaces with corrosion byproducts in no more than 5–10 years. The steady exposure to an acidic environment due to the low pH of rainwater, accelerate corrosion.[6–8]

When zinc is exposed to SO_x present in the atmosphere, sulfur gas would be dissolved into zinc surface films. The sulfur

[a]Department of Electrical and Computer Engineering, Sungkyunkwan University, Suwon 16419, Republic of Korea. E-mail: pdphong@skku.edu

[b]Interdisciplinary Program in Photovoltaic System Engineering, Sungkyunkwan University, Suwon 16419, Republic of Korea

[c]College of Information and Communication Engineering, Sungkyunkwan University, Suwon 16419, Republic of Korea. E-mail: junsin@skku.edu
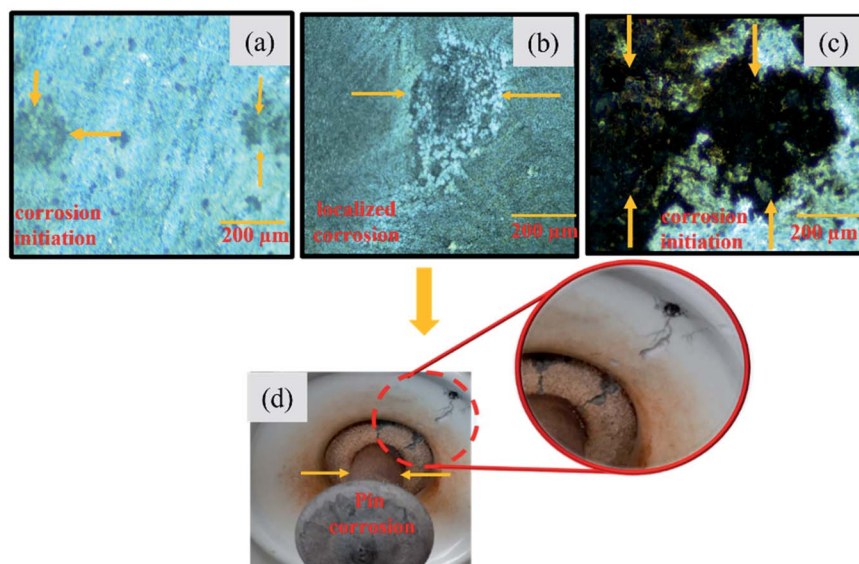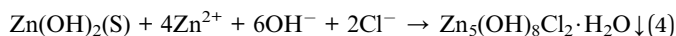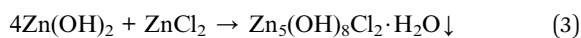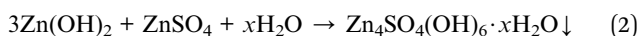
Fig. 1 The microstructural analysis of insulator pins aged more than 5 years collected from industrial sites (a) corrosion initiation, corrosion rate 10 μm per year (b) localised corrosion, corrosion rate 20 μm per year (c) severe corrosion, corrosion rate 35 μm per year (d) macroscopic analysis of crack propagation within insulator due to pin corrosion.

gas would oxidize to bisulfate, HSO_3^- eventually. Consequently, bisulfite would be converted to sulfate ion by O_3 or H_2O_2. Once sulfate is formed, it is available to form zinc hydroxy sulfates (see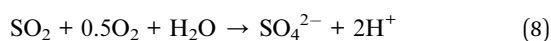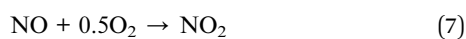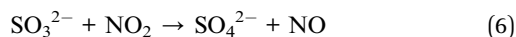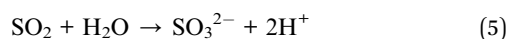 eqn (1) and (2)). The formation of zinc hydroxy sulfates is usually observed in industrial regions that are easily soluble in weak acids

$$Zn^{2+} + SO_4^{2-} + xH_2O \rightarrow Zn_4SO_4 \cdot xH_2O\downarrow \qquad (1)$$

$$3Zn(OH)_2 + ZnSO_4 + xH_2O \rightarrow Zn_4SO_4(OH)_6 \cdot xH_2O\downarrow \qquad (2)$$

$$4Zn(OH)_2 + ZnCl_2 \rightarrow Zn_5(OH)_8Cl_2 \cdot H_2O\downarrow \qquad (3)$$

$$Zn(OH)_2(S) + 4Zn^{2+} + 6OH^- + 2Cl^- \rightarrow Zn_5(OH)_8Cl_2 \cdot H_2O\downarrow (4)$$
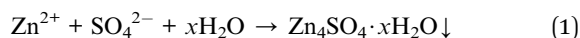
When chloride enters the zinc surface through the incorporation of gaseous HCl or deposition of salt particles, sequential combination reactions resulted in the formation of zinc hydroxy chlorides. The zinc hydroxy chlorides were easily soluble in weak acid solution (see eqn (3)–(8)). The removal of sacrificial coating (Zn) would accelerate corrosion for insulator pins.[9–11]

$$SO_2 + H_2O \rightarrow SO_3^{2-} + 2H^+ \qquad (5)$$

$$SO_3^{2-} + NO_2 \rightarrow SO_4^{2-} + NO \qquad (6)$$

$$NO + 0.5O_2 \rightarrow NO_2 \qquad (7)$$

$$SO_2 + 0.5O_2 + H_2O \rightarrow SO_4^{2-} + 2H^+ \qquad (8)$$

Corrosion of insulator pins is still controlled by conventional approaches like the application of barrier coatings like paint, plastic, and powder. Paintworks as a coating to protect insulator hardware from electrochemical charges that promote corrosion. The plastic and wax coatings are spread on insulator hardware

to increase the corrosion resistance capability of insulator hardware. Powders including epoxy, nylon, and urethane are heated to form a protective layer on insulator hardware to inhibit corrosion. The cons associated with barrier coatings is, they needed to be stripped and reapplied after a certain duration. Any damage in the paint surface led to an increased level of corrosion.[12] The volatile organic compound found in paints form the ozone layer in the surroundings when interacting with nitrogen oxide and carbon monoxide during daytime creates a threat to the environment. Implementation of corrosion-resistant alloys for pins is an expensive alternative where the adjoining metals should also be compatible. While cathodic protection is highly effective in low to a medium corrosive atmosphere. It is not effective for sites with a corrosion rate of more than 20 μm per year.[13–15] The RTV silicone coating is a recent and popular strategy utilized by the ceramic insulator industry. Nonetheless, it is an extreme threat to the eyes, inhalation system, skin, and carcinogenic. In addition, beyond their contribution to oceans and water pollution from their production and usage, synthetic polymer-based coatings are a critical challenge on land.[16]

In recent decades, consciousness regarding environmental, ecological, and health risks have developed among the present generation. This has resulted in increased attempts to develop a new series of eco-friendly and efficient green coatings to inhibit corrosion in insulators. To continue with the approach a novel, ecofriendly and efficient corrosion sealing coating is reported for insulator hardware installed in severe corrosive installation sites. The cerium is an economical, abundant, and eco-friendly metal. Cerium-based oxides were utilized for various technological applications due to the electronic structure of Ce. The Ce-based salts were reported in many applications such as electrochemical cells, UV absorbers, thermal

barriers, and microelectronics.[17–20] However, this has not been reported in any application for the high voltage insulator industry or power utilities. Here, a novel, eco-friendly and efficient, Ce-based anticorrosion sealing coating for high voltage insulators installed in severe corrosive (35 μm per year) installation sites. To keep the strategy simpler, economical, and fast, 3 step chemical conversion process is adapted for the synthesis of novel Ce-based sealing coating on insulator pin. The sealing coating bath parameters are optimized for the development of flawless, hard, self-healing, crack, and thermal resistive protective sealing coating. The characteristics of sealing coating are investigated by utilizing measurement techniques along with optical imaging (OM), scanning electron microscope (SEM), energy dispersive spectroscope (EDS), potentiodynamic corrosion test, and X-ray photoelectron spectroscopy (XPS).

2. Experimental setup

2.1 Specimen preparation

The galvanized mild steel insulator pin samples,10.7 cm in length and coated with 180 μm of zinc were employed. Multiple samples and corrosive media were considered for each set of experiments to evaluate the repeatability and reproducibility of the observed results. Before the experiment, the specimens were stripped mechanically by SiC-500 and SiC-1000 mesh papers. Consequently, it is cleaned with acetone, isopropyl alcohol (IPA), and deionized (DI) water for 10 min each in an ultrasonic bath. The pretreatment process also involves alkaline cleaning by Turco 6849 (20 volume%) at 50 °C. After that, samples were rinsed in DI water for 2 minutes. The conversion sealing coating form by the following three steps: (i) oxide growth – the specimens were immersed in an acidic solution (250 ml) containing H_2O_2 (30 vol%, 2.5 ml) and HNO_3 (65–67%, 5 ml) for 30 minutes to initiate the growth of a metal oxide structure on the metal surface. The pH of the acidic solution is 3.5. (ii) Thickening of oxide – the specimens are dipped into DI water for 30 minutes at a temperature of 90 °C. The temperature was increased to promote oxide thickening. (iii) Sealing oxide layer – the oxide sealing solution was made by dissolving 10 000 ppm–100 000 ppm $CeCl_3 \cdot 7H_2O$ (99.9%) to make a 500 ml sealing coating solution. The specimens were treated for 60 minutes in this solution at a temperature of 50 °C. The function of the sealing layer is to infuse and seal the oxide layer. Between each step of the pre-treatment and coating process, the specimens were rinsed in a DI water bath. After the coating process, the specimens were kept at room temperature for 24 h for drying in ambient air.[17–23] All the reagents used were supplied by Sigma Aldrich, Korea.

For evaluating the anticorrosion performance of Ce-based coating, bare and coated specimens were dipped in an industrial corrosive medium for 30 days at 25 °C. The corrosive solutions Sol I1 and Sol I2 were prepared by adding H_2SO_4 (95–98%, 0.5 ml), HNO_3 (65–67%, 0.3 ml), NaCl (99.0%, 6 g) and H_2SO_4 (95–98%, 1 ml), HNO_3 (65–67%, 1 ml), NaCl (99.0%, 10 g) respectively maintaining corrosion rates as 35 μm per year and 35 μm per month. All the immersion tests were performed under the conditions provided by the American Society for Testing and Materials (ASTM) G 31-72 and (ASTM) G1 standard specifications. The specification of Ce-based sealing bath and corrosive media bath is described in Table 1.

2.2 Measurements

An OM (Korean Scientific Inc. UCMOS03100KPA) and SEM equipped with an EDS (FESEM III/EDS, JSM7500F) were employed to analyze the surface morphologies and chemical configuration of the bare and coated specimens before and after exposure to corrosive media. The corrosion performance of bare and cerium-based coated specimens was evaluated by using polarization curves. The potentiostat/galvanostat model WIZEIS – 1200 PREMIUM, was employed for electrochemical experiments. A three-electrode system with electrolyte (I4) was utilized for corrosion experiments. The Ag/AgCl, platinum, and galvanized steel (specimens) were employed as a reference, counter, and working electrode sequentially. The polarization parameters were calculated by using Tafel extrapolation. The potential was scanned at 1 mV s^{-1}. The XPS was performed by employing Thermo, ESCALAB250 device. The base pressure in the UHV chamber was kept at 10^{-9} bar. The spectra were acquired at 15 kV and 20 mA with the line of Mg Kα (1253.6 eV) radiation to study the surface composition of specimens. The C 1s were considered as the reference for internal binding energy. The thickness of the specimens pre and post immersion to corrosive media was measured using an Elemetron thickness gauge meter.

3. Results and discussions

3.1 Coating synthesis

The sealing coating features were analyzed after removal from the coating bath and dried for 24 hours. The microscopic features of Ce coated insulator pins obtained after immersion in various $CeCl_3 \cdot 7H_2O$ concentration solutions are shown in Fig. 2. Fig. 2(a) and (b) present the scanned microscopic micrographs of coated insulator pins after 60 minutes immersion in 10 000 ppm and 30 000 ppm Ce salt sealing coating bath respectively. A non-uniform and flaky film were formed in both cases. This film has not covered the full surface continuously. The reason may be the insufficient concentration of $CeCl_3 \cdot 7H_2O$ in the sealing coating bath solution.[21] The experiments were performed by increasing time of immersion to 180 minutes. However, the results did not show progress even with increasing the immersion time. Fig. 2(c) depicts continuous and uniform protective film formed on the specimen surface. In the case of Fig. 2(d) the cracks can be observed on the sealing coating surface. The reason may be tension developed due to the formation of a very thicker sealing coating.[21] The strain developed within the sealing coating led to crack propagation on the coating surface. To add more insights EDS was performed. Fig. 3 presents the EDS analysis of the coated insulator pin specimens. EDS confirms the presence of Fe, Zn, Ce, O, and Cl in the sealing coating. Fig. 3(a) and (b) present the EDS analysis of specimens immersed in 10 000 ppm and 60 000 ppm sealing coating bath respectively. The weight (%) of Zn

Table 1 Composition of inhibition and corrosive media

Solutions	Type	Condition	pH	C. R.
Sol-A	Sealing coating solution	Ce/10 000 ppm/60 min	N/A	
Sol-B		Ce/30 000 ppm/60 min		
Sol-C		Ce/60 000 ppm/60 min		
Sol-D		Ce/100 000 ppm/60 min		
Sol-I1	Industrial corrosion media	H_2SO_4 (0.5 ml), HNO_3 (0.3 ml), NaCl (6 g)	5.1	35 μm per year
Sol-I2		H_2SO_4 (1 ml), HNO_3 (1 ml), NaCl (10 g)	3.2	35 μm per month

decreased by 65.7% and Ce enhanced by 84.4% with the formation of a protective sealing coating, confirm Ce enriched thick and uniform protective sealing coating for pin immersed in 60 000 ppm coating bath. Fig. 4(d) shows an increasing trend for the weight (%) of Ce, O and decreasing weight (%) of Zn with an increase in the concentration of Ce in the sealing coating bath.[21] This assures the existence of cerium-based oxides/hydroxides in the protective film formed over insulator pin specimens.

For reproducibility of the results, 5 specimens were tested for each coating condition. Further sealing coating thickness was measured for all specimens to make the process scalable. Fig. 4 presents a normal distribution plot for sealing coating thickness measured by the Elemetron thickness gauge meter. The sealing coating thickness is normally distributed. The sealing coating thickness varies from 5.1 to 38.9 μm for specimens immersed in 10 000 ppm to 100 000 ppm Ce-based sealing coating solution sequentially. For specimens immersed in a 60 000 ppm sealing coating bath, the average sealing coating thickness is 24.4 μm.

3.2 Inhibition performance of Ce based protective sealing coatings

After the sealing coating synthesis inhibition characteristics of the sealing coatings were evaluated by utilizing polarization curves. The electrochemical behavior of the cerium-based sealing coatings after immersion in industrial corrosive media (Sol-I1) for 30 days is shown in Fig. 5. The anodic and cathodic polarization branches predict the Tafel behavior of these specimens. To select the optimized concentration of cerium in the sealing coating bath, corrosion kinetic parameters at a concentration range of 10 000 ppm–100 000 ppm was evaluated and inhibition efficiencies were calculated. The maximum corrosion current density (I_{corr}) is observed for uncoated specimens. This confirms the superior corrosion resistance properties of coated pin specimens. The corrosion current density (I_{corr}) of coated specimens decreases with the increasing concentration of Ce salts in the sealing coating bath. The specimens immersed in a 60 000 ppm Ce sealing coating bath show the lowest I_{corr}. However, the I_{corr} increases when the concentration of
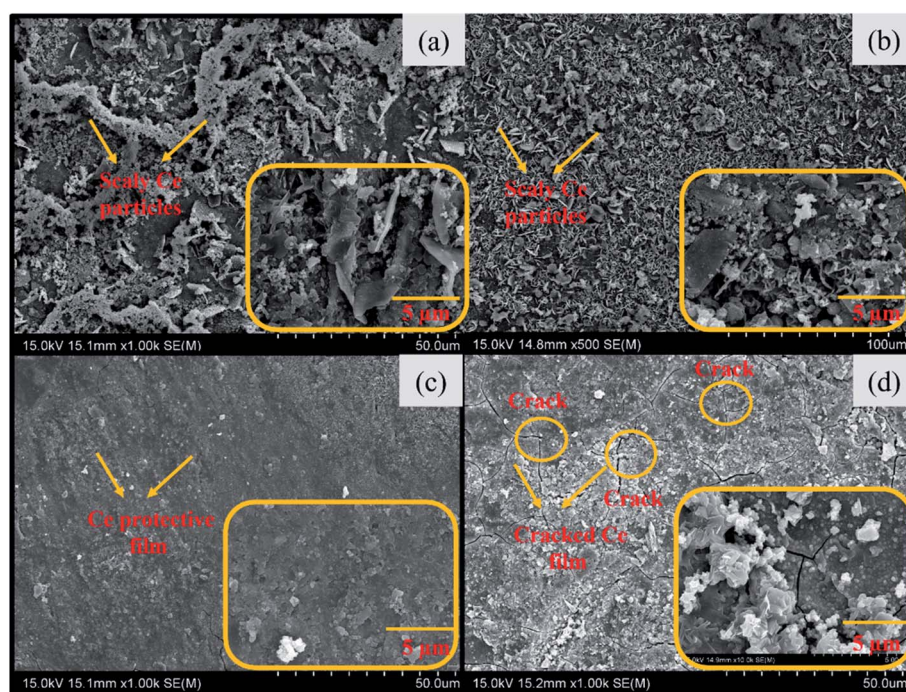

Fig. 2 Scanned micrographs of specimens immersed in cerium salts sealing coating bath (a) 10 000 ppm (b) 30 000 ppm (c) 60 000 ppm (d) 100 000 ppm.
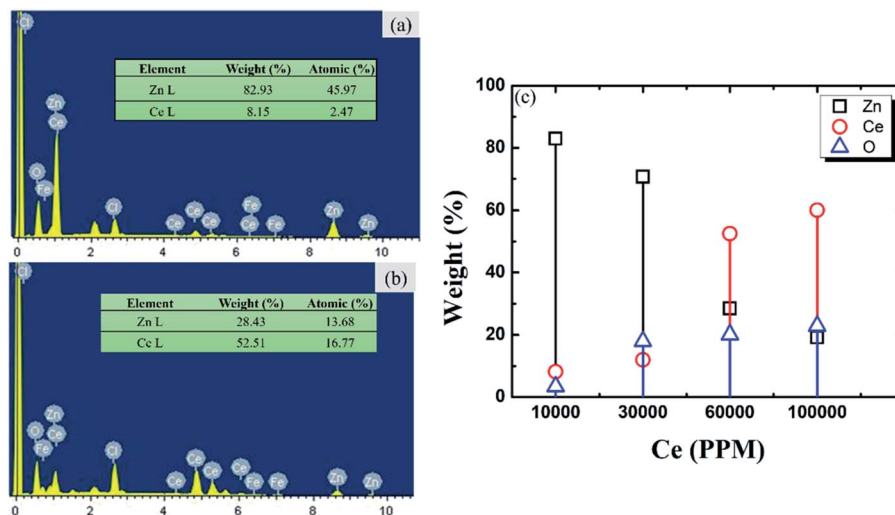
Fig. 3 EDS measurements of specimens immersed in cerium salts sealing coating bath (a) 10 000 ppm (b) 60 000 ppm (c) trend of weight (%) of Zn, Ce, and O with increasing concentration of cerium salts.
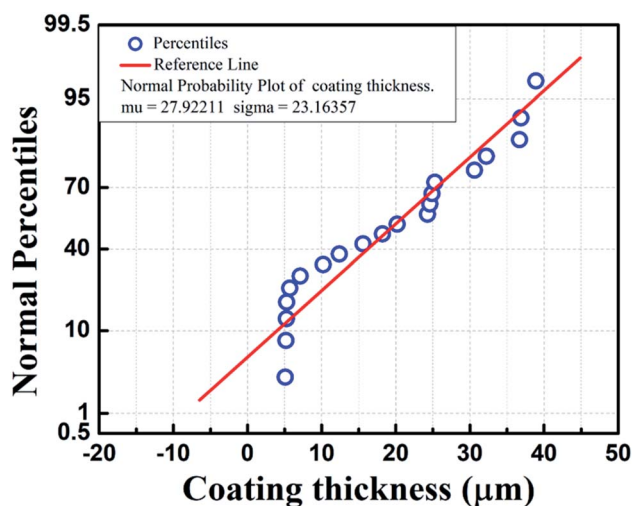

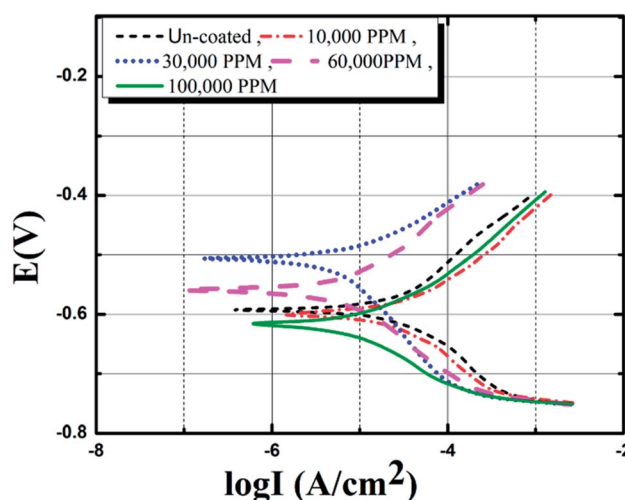**Fig. 4** Normal plot for sealing coating thickness of coated insulator pins.

Fig. 5 Tafel curves for insulator pins in industrial corrosive media.

CeCl$_3$·7H$_2$O reaches up to 100 000 ppm. This shows an excessive concentration of Ce salts added in the sealing coating bath could have degraded the crack resistance and consistency of protective sealing coating. Table 2 provide corrosion kinetic parameters of insulator pin specimens with various concentration of cerium salts in industrial corrosive media (Sol-I1). It is observed from Table 2, the corrosion current density (I_{corr}) and corrosion rate degrade by 3 times (approx.) for coated specimens concerning non-coated ones. The specimens immersed in a 60 000 ppm Ce sealing coating bath show the lowest I_{corr}, corrosion rate, and highest inhibition performance efficiency (P (%)). The inhibition performance efficiency P (%) was calculated by using the following

$$P\ (\%) = \frac{I_{\text{corr(uncoated)}} - I_{\text{corr(coated)}}}{I_{\text{corr(uncoated)}}} \qquad (9)$$

While the inhibition efficiency degrades by 1.2 times with Ce concentration increasing to 100 000 ppm. Another explanation might be after 60 minutes of immersion in 10 000 ppm and 30 000 ppm Ce salt sealing coating baths, the coated insulator pins had a non-uniform and flaky covering on the pin surface.

Table 2 Corrosion kinetic parameters of insulator pins with various concentration of cerium salts in industrial corrosive media (Sol-I1)

Quantity (ppm)	E_{corr} (V)	I_{corr} (A cm^{-2})	Corrosion rate (mm per year)	P (%)
0	−0.573	4.61×10^{-6}	5.41×10^{-2}	
10 000	−0.598	3.34×10^{-6}	3.92×10^{-2}	28.3
30 000	−0.51	1.32×10^{-6}	1.55×10^{-2}	71.37
60 000	−0.56	2.34×10^{-7}	2.80×10^{-3}	95
100 000	−0.612	1.10×10^{-6}	1.29×10^{-2}	76.08

This coating did not continuously cover the entire surface. The reason might be a lack of CeCl₃·7H₂O concentration in the sealing coating bath solution. Immersion in a 60 000 ppm coating bath solution for 60 minutes demonstrates the formation of a continuous and homogeneous protective layer on the specimen surface. With the creation of a protective sealing coating, the weight (%) of Zn reduced by 65.7% and Ce increased by 84.4% (Fig. 3(b)), confirming Ce enriched thick and uniform protective sealing coating for pin submerged in 60 000 ppm coating bath. However, fractures on the sealing coating surface can be seen after immersion in a 100 000 ppm coating bath solution. The cause might be strain caused by the creation of a much thicker sealing layer. As a result, immersion in a 60 000 ppm coating bath solution for 60 minutes results in the lowest I_{corr} (2.8 × 10⁻³).

To obtain more details on the inhibition properties of Ce-based sealing coating, XPS studies were performed for specimens post immersion in industrial corrosive media (Sol-I1). Fig. 6(a) represents the survey spectra for both bare and coated specimens. The main elements detected for coated specimens were Zn, Ce, Cl, Na, and C. However, for non-coated specimens, the main elements are Zn, Cl, Na, C, and S.[22-23] The presence of carbon in both specimens is due to the presence of CO₂ in the atmosphere. The Zn 2p peak (Fig. 6(b)), associated at binding energy 1045.7 eV, and 1022.01 eV depicts ZnO type compound in specimens. Similarly, the Zn 3s peak at 140.09 eV also depicts the presence of ZnO or ZnO type compound in specimens. The O 1s display overlapped peaks indicating the presence of both zinc–oxygen and cerium–oxygen at 532.16 eV.

In the case of coated specimens, the O 1s peak (532.2 eV) may contribute to cerium-oxides/cerium hydroxylated compounds. However, for bare specimens, it indicates the presence of ZnO (531.5 ± 1 eV). The first peak corresponding to Ce 3d (Fig. 6(c)), at binding energy 881.45 eV indicates Ce₂O₃. The second peak corresponded to Ce 3d₅/₂ spectra having binding energies 881.7 ± 0.5 eV may indicate CeO₂. The peak at 917 eV predicts the presence of CeO₂ again. Comparing the theoretical Ce spectra values reported in the literature it can be suggested that Ce(OH)₃, CeO₂, and Ce₂O₃ were found in the Ce coated specimens.[22] Fig. 6(b) and (c) also indicate the existence of minimum intensity of ZnO and maximum intensity of Ce compounds on the protective film for specimens immersed in 60 000 ppm sealing coating bath post immersion to Sol-I1 for 30 days. Thus, ensures the highest inhibition efficiency. The XPS studies also confirm the presence of cerium compounds on all coated pin surfaces post immersion in industrial media (Sol-I1) for 30 days. Fig. 6(d) indicates with the increase in the concentration of Ce to 60 000 ppm in the sealing coating bath, the atomic weight (%) of Ce increased from 2.08 to 12.42 indicating the formation of insoluble cerium compounds on the pin surface. However, excessive concentration of Ce in the sealing coating bath would result in cracks in the protective film. Thus, reducing the corrosion resistance of the protective film.

3.3 Activity of protective sealing coating towards scratched surface

To evaluate the activity of sealing coating towards scratched surface, the specimens showed excellent inhibition
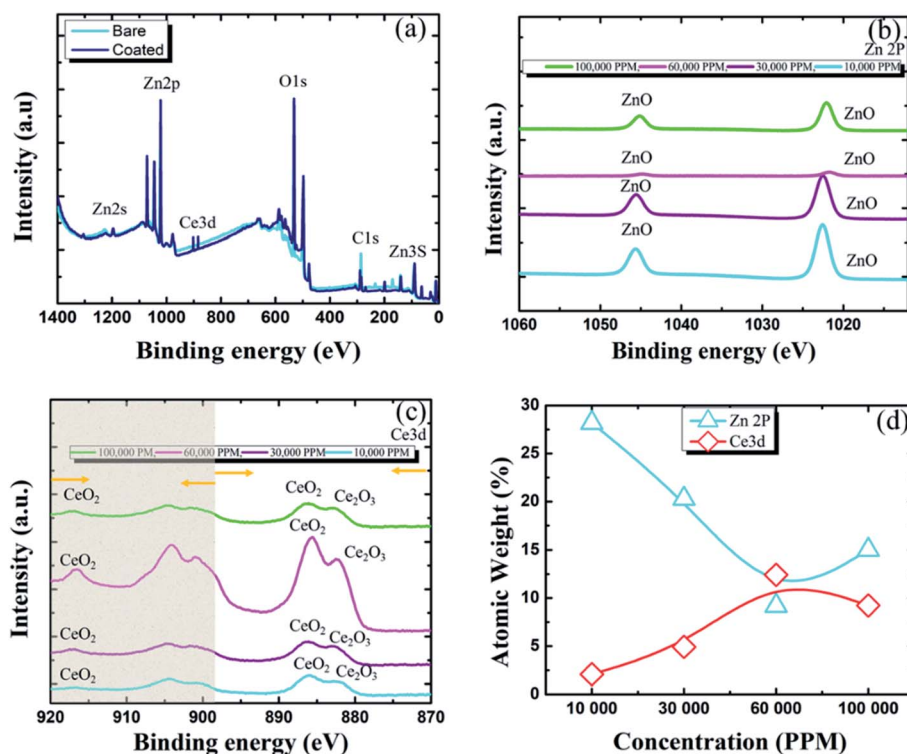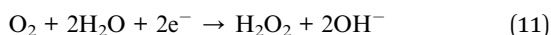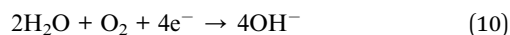

Fig. 6 Results of XPS analysis post immersion in industrial corrosive media, Sol-I1 for 30 days (a) survey spectra of bare and coated pin specimens (b) narrow spectra of Zn 2P (c) narrow spectra of Ce 3d (d) atomic weight (%) of zinc and cerium present in the protective sealing coating.

performance (60 000 ppm) was investigated by XPS, with and without manual scratch post immersion in industrial corrosive media Sol-I1. O 1s spectra shown in Fig. 7, indicate an increase in the intensity of Ce-hydroxylated, Ce(III) and Ce(IV) groups for scratched specimens concerning unscratched specimens post immersion in Sol-I2. After contact between electrolyte and pin specimens, the following reaction occurs.
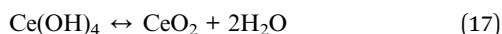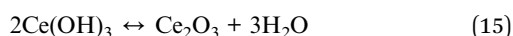
Cathode:

$$2H_2O + O_2 + 4e^- \rightarrow 4OH^- \tag{10}$$

$$O_2 + 2H_2O + 2e^- \rightarrow H_2O_2 + 2OH^- \tag{11}$$

$$H_2O_2 + 2e^- \rightarrow 2OH^- \tag{12}$$

Anode

$$Zn \rightarrow Zn^{2+} + 2e^- \tag{13}$$

The reaction of the OH^- ions with Ce(III) and Ce(IV) ions existing in the sealing coating[23,24]

$$Ce^{3+} + 3OH \rightarrow Ce\,(OH)_3 \tag{14}$$

$$2Ce(OH)_3 \leftrightarrow Ce_2O_3 + 3H_2O \tag{15}$$

$$Ce^{4+} + 4OH^- \rightarrow Ce(OH)_4 \tag{16}$$

$$Ce(OH)_4 \leftrightarrow CeO_2 + 2H_2O \tag{17}$$

The indissoluble Ce species, observed in the XPS study are responsible for the curing of cerium-based protective film. Similar studies were reported for PMMA-silica hybrid coating modified with various concentrations of Ce(IV) ions for carbon steel, PMMA-silica hybrid coating developed on mild steel, silane coatings modified by CeO_2 nanoparticles, and Ce(III) ions developed on steel alloy.[23,24]
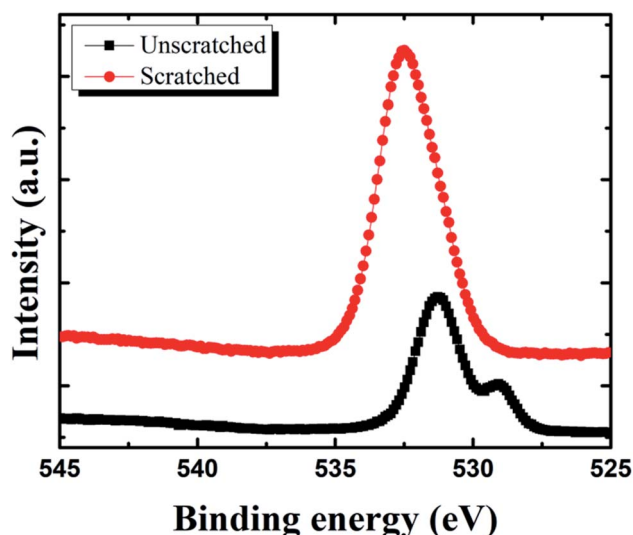
3.4 Surface analysis

The surface analysis of uncoated and coated specimens (60 000 ppm), post immersion in industrial corrosive media (Sol-I2) is investigated in this section. The specimens immersed in corrosive media (Sol-I2) accelerated the corrosion phenomenon seems to occur in a year by using Sol-I1, to a month. The Sol-I2 was used to understand the surface-morphological changes in detail.

As a complementary confirmation technique galvanized layers of pin specimens were measured after exposure to corrosion media (Sol-I2) for both bare and coated specimens to confirm the inhibition efficiency of the proposed sealing coating. Fig. 8 presents results of galvanized coating thickness for both bare and coated specimens, post immersion to corrosion media (Sol-I2). During 1–4 weeks of exposure to corrosion media, the bare galvanized pin specimens present 35.2 μm of coating loss. Under such an extremely corrosive environment the lifetime of the galvanized layer would be 5.1 years only. However, the optimized coated specimens present almost negligible coating loss after exposure to corrosive media for 4 weeks. The coated specimens depict 40 times (approx.) better corrosion protection to insulator pins concerning uncoated galvanized insulator pins.

Fig. 9 presents the macrographs and micrographs of uncoated pin specimens, post immersion to corrosive media for 30 days. The SEM results are in line with coating thickness measurement results for pin specimens. After 7 days the uncoated specimen comprises faded metallic luster and minor signs of dissolution of top Zn layer at some sites as presented in Fig. 9(a) and (e). After 14 and 21 days of immersion, most of the metallic luster faded away with major signs of dissolution of galvanized coating as shown in Fig. 9(b) and (c). The micrographs of the corresponding specimen present pitting/localized corrosion after 21 days of immersion as shown in Fig. 9(g). After the exposure time exceeds 30 days the specimen shows significant corrosion. The pin surface lost all the metallic luster and
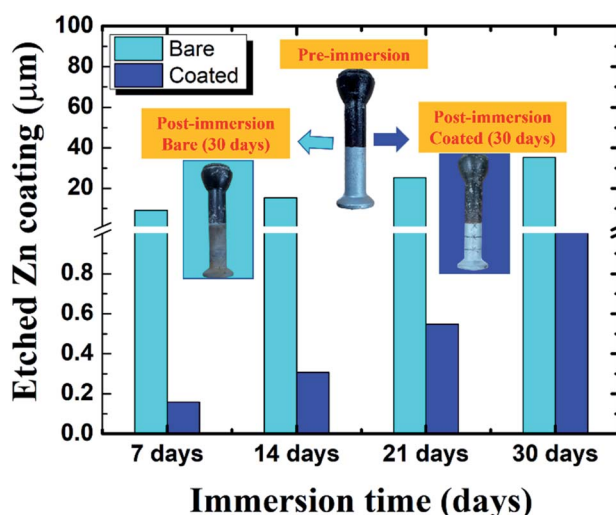

Fig. 7 XPS O 1s spectra of unscratched and scratched specimens immersed in industrial corrosive media.

Fig. 8 Measurement of coating thickness for bare and coated pin specimens (60 000 ppm) post immersion to corrosive media (Sol-I2).
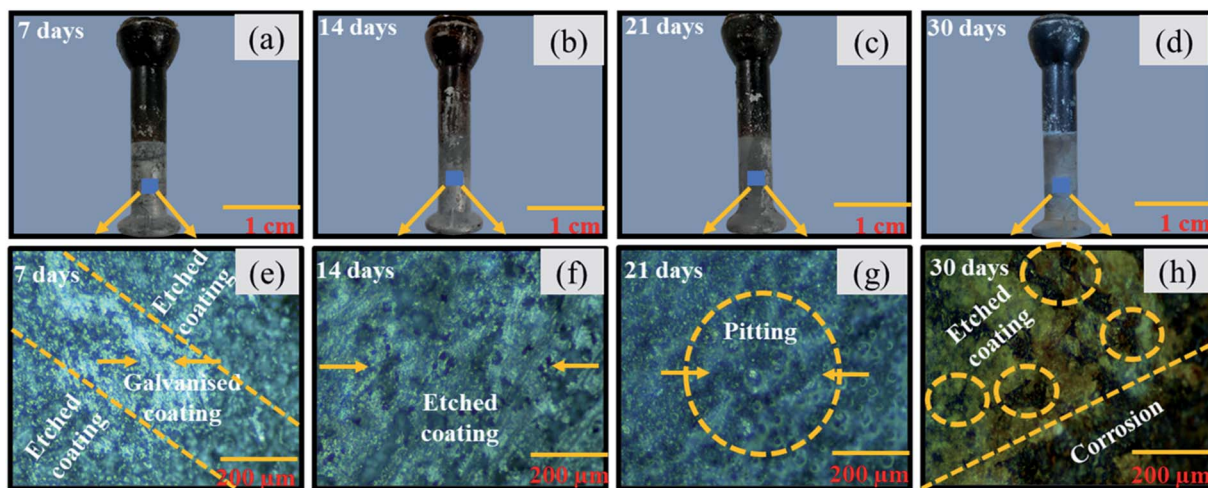
Fig. 9 Optical macro and micro graphs for uncoated pin specimens post immersion in industrial corrosive media for (a) 7 days (b) 14 days (c) 21 days (d) 30 days (e) 7 days (f) 14 days (g) 21 days (h) 30 days.
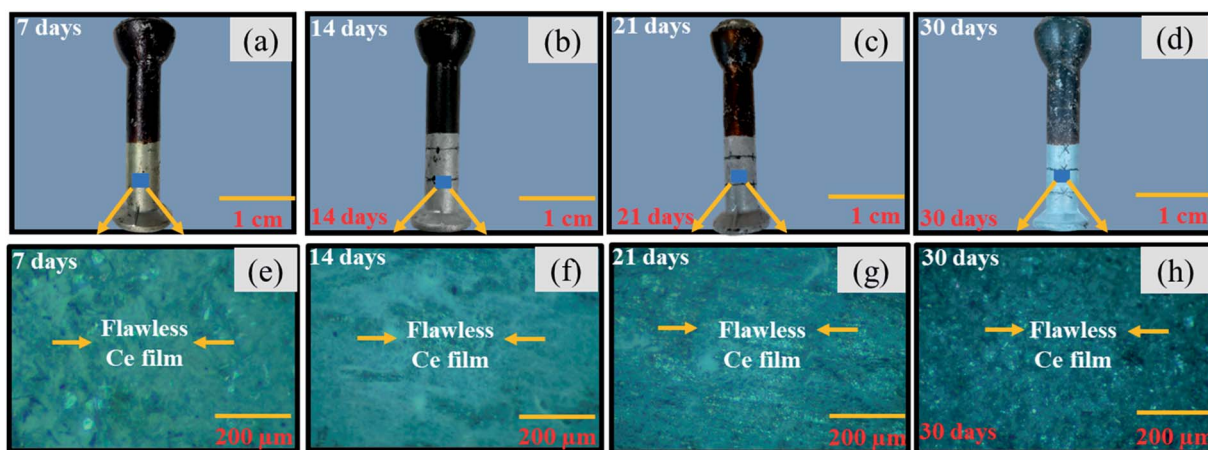

Fig. 10 Optical macro and micro graphs for coated pin specimens (60 000 ppm) post immersion in industrial corrosive media for (a) 7 days (b) 14 days (c) 21 days (d) 30 days (e) 7 days (f) 14 days (g) 21 days (h) 30 days.

faded to brown color. The dark brown colored corrosion products spread on the pin surface as shown in Fig. 9(d) and (h).

Fig. 10 presents the macrographs and micrographs of coated pin specimens post immersion to corrosive media for 30 days. It can be seen from Fig. 10(a) and (e) that even after 7 days of exposure to corrosive media, the yellow protective film developed on the pin surface initially after sealing the coating does not show any damage or color change. After 14, 21, and 30 days of exposure as shown in Fig. 10(b)–(h) the yellow color sealing coating of specimens transformed to milky white and finally to transparent white. The simultaneous redox reactions may be the reason for color change. No significant etching of the protective sealing coating or initiation of corrosion is observed in the coated specimens.

The morphology of the coated specimens was further studied with SEM. Fig. 11 depicts micrographs of the coated specimen after 30 days of exposure to corrosive media (Sol-I2). The SEM micrographs are also in agreement with the previous results. Any sign of coating damage, crack or the initiation of corrosion process is not observed for coated pin specimens in Fig. 11.

The proposed sealing coating has been synthesized uniquely and has not been used for insulators previously. Due to its high melting point (1060 K), low thermal conductivity (2 W mK^{-1}), high crack resistance and easily tailored structure the proposed sealing coating have a high potential to function as sealing coating material for insulator pin as well as all-metal accessories used in power utilities in future.[25] This work would pave the way to utilize cerium-based eco-friendly and highly efficient coatings for high voltage insulator and power industries.

4. Conclusion

In this study, the anti-corrosion performance of sealing coating against corrosion has been investigated. The immersion of specimens for 60 minutes in a 60 000 ppm Ce salt sealing
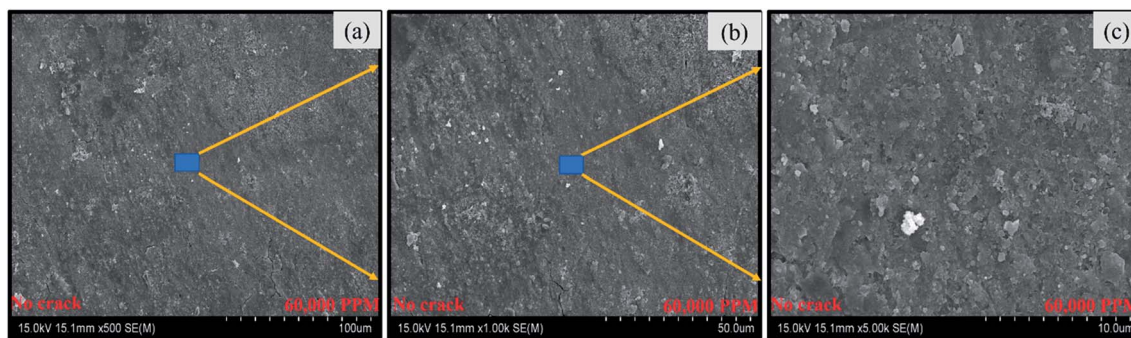
Fig. 11 SEM micrographs of coated specimens (60 000 ppm) post exposure to corrosion media (Sol-I2) at various magnifications (a) 500× (b) 1000× (c) 5000×.

coating bath developed a uniform and continuous protective film over the pin surface unlike those immersed for 60 minutes in 10 000 ppm and 30 000 ppm sealing coating bath. The specimen immersed in a 100 000 ppm sealing coating bath for 60 minutes showed cracks in the protective film because of tension developed due to the formation of a very thicker sealing coating. The EDS reveals the weight (%) of Zn decreased by 65.7% and Ce enhanced by 84.4% with the formation of a protective sealing coating, confirming Ce enriched thick and uniform protective sealing coating for pin immersed in 60 000 ppm sealing coating bath. The increasing trend for the weight (%) of Ce, O and decreasing weight (%) of Zn with an increase in the concentration of Ce in the sealing coating bath, assure the existence of cerium-based oxides/hydroxides in the protective film formed over the insulator pin specimens. The sealing coating thickness varies from 5.1 to 38.9 μm for specimens immersed in 10 000 ppm to 100 000 ppm Ce-based sealing coating solution sequentially. For specimens immersed in a 60 000 ppm sealing coating bath, the average sealing coating thickness is 24.4 μm. The polarization curves confirm the specimens immersed in 60 000 ppm Ce sealing coating bath show the lowest I_{corr}, corrosion rate, and highest inhibition performance efficiency. While the inhibition efficiency degrades by 1.2 times with Ce concentration increasing to 100 000 ppm. The XPS confirms the existence of $Ce(OH)_3$, CeO_2, and Ce_2O_3 in the protective sealing film. Further, it indicates the existence of minimum intensity of ZnO and maximum intensity of Ce compounds on the protective film for specimens immersed in 60 000 ppm sealing coating bath post immersion to industrial corrosion media (Sol-I1) for 30 days. Thus, ensures the highest inhibition efficiency of the specimen. The indissoluble Ce species, observed in the XPS study for manually scratched specimens are responsible for the self-healing property of cerium-based sealing film. The thickness gauge meter confirms during 1–4 weeks of exposure to corrosion media, the bare galvanized pin specimens present 35.2 μm of coating loss. However, the optimized coated specimens present almost negligible coating loss after exposure to corrosive media for 4 weeks. The measurement suggests, the coated specimens depict 40 times (approx.) better corrosion protection to insulator pins concerning uncoated galvanized insulator pins. The micrographs revealed the bare pin specimens, lost most of the metallic luster and major signs of dissolution and pitting of galvanized coating after 14 and 21 days of immersion, unlike coated specimens. Any sign of coating damage, crack or the initiation of corrosion process is not observed for coated pin specimens. Thus, it can be concluded that due to the combination of inhibition efficiency, self-healing ability, economical, and eco-friendliness Ce-based sealing coatings are promising alternatives to silicone coatings for extending the service life of insulators.

Conflicts of interest

There are no conflicts of interest to declare.

Acknowledgements

References

1 L. Luo, L. Wang, Z. Guan, F. Zhang and L. Li, Influence of pin corrosion on mechanical characteristic of UHVDC disc suspension insulators and solutions, *IEEE Trans. Dielectr. Electr. Insul.*, 2015, **22**(4), 2242–2251, DOI: 10.1109/TDEI.2015.005053.

2 Z. Pei, *et al.*, Understanding environmental impacts on initial atmospheric corrosion based on corrosion monitoring sensors, *J. Mater. Sci. Technol.*, 2021, **64**, 214–221, DOI: 10.1016/j.jmst.2020.01.023.

3 D. Thierry, N. LeBozec, A. Le Gac and D. Persson, Long-term atmospheric corrosion rates of hot dip galvanised steel and zinc-aluminium-magnesium coated steel, *Mater. Corros.*, 2019, **70**(12), 2220–2227, DOI: 10.1002/maco.201911010.

4 R. Vera, R. Araya, C. Garín, S. Ossandón and P. Rojas, Study on the effect of atmospheric corrosion on mechanical properties with impact test: Carbon steel and Galvanized steel, *Mater. Corros.*, 2019, **70**(7), 1151–1161, DOI: 10.1002/maco.201810666.

5 E. Almeida, M. Morcillo and B. Rosales, Atmospheric corrosion of zinc Part 1: Rural and urban atmospheres, *Br.*

Corros. J., 2000, **35**(4), 284–288, DOI: 10.1179/000705900101501353.

6 F. Corvo, J. Reyes, T. Pérez and A. Castaeda, *Role of NO_x in materials corrosion and degradation*, Centro Nacional de Investigaciones Científicas de Cuba, 2010, vol. 41, pp. 1–10, https://www.redalyc.org/pdf/1816/181620500032.pdf.

7 M. Mouanga, P. Berçot and J. Y. Rauch, Comparison of corrosion behaviour of zinc in NaCl and in NaOH solutions. Part I: Corrosion layer characterization, *Corros. Sci.*, 2010, **52**(12), 3984–3992, DOI: 10.1016/j.corsci.2010.08.003.

8 S. Wu, H. Chen, H. L. Ramandi, P. C. Hagan, A. Crosky and S. Saydam, Effects of environmental factors on stress corrosion cracking of cold-drawn high-carbon steel wires, *Corros. Sci.*, 2018, **132**, 234–243, DOI: 10.1016/j.corsci.2017.12.014.

9 G. Hölzl, G. Luckeneder, H. Duchaczek, C. Kleber and A. W. Hassel, Evolution and interaction of corrosive species during the initial NaCl particle induced corrosion on zinc coated skin-passed steel, *Corros. Sci.*, 2017, **127**, 222–229, DOI: 10.1016/j.corsci.2017.08.001.

10 S. Liu, X. Zhao, H. Zhao, H. Sun and J. Chen, Corrosion performance of zinc coated steel in seawater environment, *Chin. J. Oceanol. Limnol.*, 2017, **35**(2), 423–430, DOI: 10.1007/s00343-016-5269-9.

11 T. Kim, Y. J. Lee, S. Sanyal, J.-W. Woo, I.-H. Choi and J. Yi, Mechanism of corrosion in porcelain insulators and its effect on the lifetime, *Appl. Sci.*, 2020, **10**(1), DOI: 10.3390/app10010423.

12 S. Sanyal, *et al.*, Influence of Corrosion on Electrical and Mechanical Properties of Porcelain Suspension Insulators: An Overview, *Transactions on Electrical and Electronic Materials*, 2020, **21**(6), 543–549, DOI: 10.1007/s42341-020-00239-3.

13 P. Pandey and U. V. Kiran, Degradation of Paints and Its Microbial Effect on Health and Environment, *J. Crit. Rev.*, 2020, 7(19), 4879–4884.

14 B. Yilmaz, H. Terekeci, S. Sandal, *et al.*, Endocrine disrupting chemicals: exposure, effects on human health, mechanism of action, models for testing and strategies for prevention, *Rev. Endocr. Metab. Disord.*, 2020, **21**, 127–147, DOI: 10.1007/s11154-019-09521-z.

15 K. L. Alford and N. Kumar, Pulmonary Health Effects of Indoor Volatile Organic Compounds—A Meta-Analysis, *Int. J. Environ. Res. Public Health*, 2021, **18**(4), 1578, DOI: 10.3390/ijerph18041578.

16 M. Campanale, L. Savino and V. F. Uricchio, A Detailed Review Study on Potential Effects of Microplastics and Additives of Concern on Human Health, *Int. J. Environ. Res. Public Health*, 2020, **17**(4), 1212, DOI: 10.3390/ijerph17041212.

17 M. Gobara, A. Baraka, R. Akid and M. Zorainy, Corrosion protection mechanism of Ce4+/organic inhibitor for AA2024 in 3.5% NaCl, *RSC Adv.*, 2020, **10**(4), 2227–2240, DOI: 10.1039/c9ra09552g.

18 M. A. Arenas, M. Bethencourt, F. J. Botana, J. De Damborenea and M. Marcos, Inhibition of 5083 aluminium alloy and galvanised steel by lanthanide salts, *Corros. Sci.*, 2001, **43**(1), 157–170, DOI: 10.1016/S0010-938X(00)00051-2.

19 M. F. Montemor, A. M. Simões and M. G. S. Ferreira, Composition and corrosion behaviour of galvanised steel treated with rare-earth salts: The effect of the cation, *Prog. Org. Coat.*, 2002, **44**(2), 111–120, DOI: 10.1016/S0300-9440(01)00250-8.

20 A. Amadeh, B. Pahlevani and S. Heshmati-Manesh, Effects of rare earth metal addition on surface morphology and corrosion resistance of hot-dipped zinc coatings, *Corros. Sci.*, 2002, **44**(10), 2321–2331, DOI: 10.1016/S0010-938X(02)00043-4.

21 P. Rodič and I. Milošev, The influence of additional salts on corrosion inhibition by cerium (III) acetate in the protection of AA7075-T6 in chloride solution, *Corros. Sci.*, 2019, **149**(10), 108–122, DOI: 10.1016/j.corsci.2018.10.021.

22 M. A. Arenas and J. J. de Damborenea, Surface characterization of cerium layers on galvanised steel, *Surf. Coat. Technol.*, 2004, **187**(2–3), 320–325, DOI: 10.1016/j.surfcoat.2004.02.033.

23 A. Trentin, S. V. Harb, M. C. Uvida, K. Marcoen, S. H. Pulcinelli, C. V. Santilli, H. Terryn, T. Hauffman and P. Hammer, Effect of Ce(III) and Ce(IV) ions on the structure and active protection of PMMA-silica coatings on AA7075 alloy, *Corros. Sci.*, 2021, **189**, 109–581, DOI: 10.1016/j.corsci.2021.109581.

24 S. V. Harb, A. Trentin, T. A. C. de Souza, M. Magnani, S. H. Pulcinelli, C. V. Santilli and P. Hammer, Effective corrosion protection by eco-friendly self-healing PMMA-cerium oxide coatings, *Chem. Eng. J.*, 2020, **383**, 123–219, DOI: 10.1016/j.cej.2019.123219.

25 C. E. Castano, M. J. O'Keefe and W. G. Fahrenholtz, Cerium-based oxide coatings, *Curr. Opin. Solid State Mater. Sci.*, 2015, **19**(2), 69–76, DOI: 10.1016/j.cossms.2014.11.005.